Gate-Voltage Control of Oxygen Diffusion on Graphene

Alejandro M. Suarez, Ljubisa R. Radovic, Ezra Bar-Ziv, and Jorge O. Sofo

Phys. Rev. Lett. **106**, 146802 — Published 5 April 2011

DOI: 10.1103/PhysRevLett.106.146802

Gate Voltage Control of Oxygen Diffusion on Graphene

Alejandro M. Suarez[1], Ljubisa R. Radovic[2,3], Ezra Bar-Ziv[4] and Jorge O. Sofo[1,5,*]

[1]*Department of Physics, Penn State University, University Park, PA 16802, USA*
[2]*Department of Energy and Mineral Engineering, Penn State University, University Park, PA 16802, USA*
[3]*Department of Chemical Engineering, University of Concepción, Concepción, Chile*
[4]*Ben-Gurion University of the Negev, Beer-Sheva, Israel*
[5]*Materials Research Institute, Penn State University, University Park, PA 16802, USA*

We analyze the diffusion of oxygen atoms on graphene and its dependence on the carrier density controlled by a gate voltage. We use density functional theory to determine the equilibrium adsorption sites, the transition state, and the attempt frequency for different carrier densities. The ease of diffusion is strongly dependent on carrier density. For neutral graphene, we calculate a barrier of 0.73 eV; however, upon electron doping the barrier decreases almost linearly to reach values as low as 0.15 eV for densities of -7.6×10^{13} cm^{-2}. This implies an increase of more than nine orders of magnitude in the diffusion coefficient at room temperature. This dramatic change is caused by a combined effect of bonding reduction in the equilibrium state and bonding increase at the transition state and can be used to control the patterning of oxidized regions by an adequate variation of the gate voltage.

PACS: 73.22.Pr, 73.22.Wp, 68.47.Gh

(*) Corresponding author: sofo@psu.edu

The two-dimensional nature of graphene is at the core of many of its extraordinary properties. In particular, chemisorbed or physisorbed atoms can influence its electronic properties and the carrier density, n, can be modified with an external gate voltage. Adatoms bind to p_z orbitals that form the bands close to the Fermi level. Electron and hole doping levels up to $|n| \approx 10^{13}$ cm^{-2} are possible with the most common gate made of a thin layer of SiO_2 grown on a Si wafer [1]. Even higher doping levels are possible with gates composed of ionic liquids [2] or $SrTiO_3$ [3]. In contrast to the more traditional chemical doping methods, gate voltage doping can be changed "on the fly" during device operation. The effects of adatoms and gate voltage on transport properties of graphene have been thoroughly studied in recent years [4, 5].

In this Letter we show that the diffusivity of oxygen on graphene can be increased at least by *nine orders of magnitude* with the application of an achievable gate voltage. Deposition patterning of adatoms can thus be controlled by manipulating their mobility on the surface. The case of oxygen is particularly important because of the relevance of graphene oxide to the physics and applications of graphene [6-9], the optical properties of carbon nanotubes [10], as well as the influence of mobile oxygen-containing surface complexes on the reactivity of both flat and curved sp^2-hybridized carbon materials [11].

The literature on oxygen diffusion, especially comparisons between theory and experiment, is quite limited for carbon surfaces. In a pioneering study, Yang and Wong [12] used etch-decoration transmission electron microscopy to obtain direct evidence for surface diffusion of oxygen on graphite and an estimate of 1.5 eV for the activation energy of site-to-site hopping. Perhaps of greatest practical relevance is the phenomenon of oxygen spillover [13-16]. It is well documented that H atoms 'jump' through the gas phase [17-19]; a similar spillover mechanism

has been invoked for oxygen atoms, although the evidence for it is much less compelling [20, 21]. Our interest in the diffusion of atomic species on the graphene surface, rather than O_2, stems from the well-known fact that chemisorbed oxygen dissociates on the surface of carbon materials [12, 22, 23]; furthermore, among the fates of molecular oxygen reversibly adsorbed on aromatics and thus forming endoperoxides [24, 25] is the formation of a di-epoxide [24].

Our electronic structure calculations were done on a periodic hexagonal supercell of 5x5 graphene unit cells, within the framework of DFT with a plane wave basis set as implemented in the VASP code [26, 27]. The in-plane lattice constant is 12.3 Å and the spacing between graphene planes was 20 Å. This supercell contains 50 C atoms and 1 O atom. As described below, our results are robust with respect to cell size. The energy cutoff was 300 eV. The core electrons are treated with the frozen core projector augmented wave (PAW) method [28, 29]. The exchange and correlation of electrons was treated with the Perdew, Burke, and Ernzerhof representation of the generalized gradient approximation (GGA-PBE) [30, 31]. The Brillouin zone was sampled with a Monkhorst-Pack [32] 5x5x1 grid with a k-point spacing of 0.019 $Å^{-1}$. Self-consistent electronic iterations were run until energy differences fell below $<10^{-5}$ eV. Atomic relaxations were run until all forces fell below 10^{-2} eV/Å. Transition states were found using the VTST [33, 34] implementation of the Nudged Elastic Band (NEB) method with 9 images. Spring constants between images were set to -5.0 $eV/Å^2$. For density of states calculations we increased the sampling of the Brillouin zone to a 20x20x1 grid. We simulated charge addition or removal by adjusting the number of electrons in the cell. Monopole and dipole corrections [35, 36] were evaluated to improve convergence with respect to the size of the cell; this was necessary due to the dipole moment generated, even in the neutral cell [37].

For all the charged states of the graphene plane (see Fig. 1 and Table I), the equilibrium position for an O atom is the epoxy configuration and the transition state is close to the top site on top of a C atom in graphene; the two C atoms bonded to O change their hybridization from sp^2 to sp^3 and pucker out of the graphene plane. In the transition state, the C atom bonded to O adopts an sp^3 hybridization producing some puckering as well. The results for the neutral system are discussed first, and are then contrasted with those obtained for the charged systems.

In the equilibrium state, the C-C bond below the adsorbed O atom is stretched to 1.51 Å, in agreement with other theoretical results [7, 38, 39] and implying no unzipping of graphene. Li et al. [6] considered a coronene molecule and found the C-C bond below the epoxy O atom to be stretched to 1.58 Å. This larger value is probably due to the extra flexibility and deformation allowed by the coronene molecule, in contrast to that of a more delocalized graphene aromaticity simulated here using periodic boundaries. The transition state obtained with the NEB method corresponds to a bound state whose position is very close to the top site with a slight tilt in the direction of one of the hexagonal holes of the graphene lattice. This tilting is apparent when we observe the three angles reported in Table I. One of these three angles is $\approx 108^{o}$ while the other two are $\approx 100^{o}$. The C-O distance is slightly shorter than in the equilibrium configuration, 1.44 *vs.* 1.49 Å. Both numbers are within the typical range for C-O single bonds [40]. The energy difference between the equilibrium and transition state is 0.73 eV for the neutral cell. The energy as a function of the path between equilibrium states, passing through the transition state, is shown in Fig. 2.

One of the peculiarities of graphene is that the carrier density can be adjusted by changing the gate voltage of the field effect transistor (FET) device. To simulate this effect, we add or

remove electrons from the cell and search for the equilibrium and transition states under such gated conditions. We tested three charged configurations corresponding to $+7.64\times10^{13}$ cm^{-2}, -3.82×10^{13} cm^{-2}, and -7.64×10^{13} cm^{-2}, corresponding to one electron removed, half electron added, and one electron added to the cell, respectively. The respective geometries and adsorption energies are reported in Table I. A most surprising result is the dramatic effect on the diffusion barrier, as shown in Fig. 2: the barrier decreases almost linearly with charge density to reach a value of 0.15 eV for the largest electron doping case tested. This in turn increases the diffusion coefficient by orders of magnitude (see below). Of great interest is to analyze the bonding changes produced by such doping.

The C-O bond distance (see Table I) shows the opposite behavior in the equilibrium state *vs*. the transition state upon increasing the electron density. In the equilibrium state, the C-O distance increases as the number of electrons increases. The barrier reduction is thus a combined effect of a weaker C-O bond in the equilibrium state and a stronger C-O bond in the transition state. There is additional evidence for both effects. The weakening of O bonding in the equilibrium state upon increasing the number of electrons is also manifested as a correlated reduction of the C-C distance between the atoms bonded to O. As the C-O bond weakens, the C-C bond tends to the pure graphene bond length. In the transition state, the C-O bond becomes stronger as electron doping increases. The three angles become similar and larger on average, indicating a stronger and more covalent bond with symmetric tetrahedral coordination. As we increase the electron doping of the cell, the equilibrium state thus becomes less bonded with an increased ionic character while the bonding of transition state becomes stronger as its covalent character increases. Although the bonding in the epoxy configuration becomes weaker, the energy per oxygen in both equilibrium and transition states remains more than 1 eV lower than

that for desorbed atomic oxygen. (Desorbed O is the appropriate reference state here, rather than O_2; the latter adsorbs dissociatively only on graphene edges and not on the basal plane [11, 12].)

Bond populations [41] further support these observations. Increasing the number of electrons, the C-O bond population in the equilibrium state decreases from 0.33 to 0.27; conversely, in the transition state the C-O bond population *increases* from 0.49 to 0.55. The densities of states (Fig. 3) provides the explanation. In the equilibrium state for the neutral case (panel 3a), the states projected on the oxygen site just above the Fermi level are mainly the antibonding states of the combination between the p_z orbitals of O and the p_z orbitals of the carbon atoms bonded to it. When electrons are added, these states become occupied (panel 3c) and the bond becomes weaker; the other p orbitals of O form a narrow band more than 2 eV below the Fermi level. In the transition state (panels 3b and 3d) , the O atom is on top of a C atom. This generates a bonding state that is a combination of the O p_z orbital and the three p_z orbitals of the carbon atoms nearest to the carbon attached to O. This produces a sharp peak close to the Fermi level; the peak is above the Fermi level when the graphene is neutral (panel 3b). It carries only part of the spectral weight of this bonding combination; the rest is at lower energies between -2 and -6 eV. The perpendicular O p states form a narrow peak with full spectral weight just below the Fermi level. When the electron density is increased (panel 3d), the Fermi level moves into the unoccupied sharp peak, the bond of O with the plane becomes stronger and because of this narrow peak the system develops a small magnetic moment of the order of $\approx 0.2\,\mu_B$ distributed between the O atom and the three adjacent carbon. A clear picture thus emerges for the cause of the reduced diffusion barrier when graphene is negatively charged with a gate voltage.

Oxygen diffusivity is strongly affected by energy barrier changes. The relevant equation is $D = d^2 \nu_0 \exp(-\Delta E / k_B T)/4$: here d is the jump length (taken to be 1.23 Å, the distance between epoxide sites) and ν_0 is the attempt frequency, calculated in the harmonic approximation [42] using the vibrational modes of the equilibrium and transition states [43]. For the neutral case, we obtain $\nu_0 = 26$ THz, in reasonable agreement with Yang and Wong [12]; with these values, the diffusivity at 300 K is 5.4×10^{-16} cm^2/s. At the same temperature and assuming the same attempt frequency, for graphene whose carrier density is increased to -7.64×10^{13} cm^{-2} the barrier is reduced to 0.15 eV (3.0×10^{-6} cm^2/s). Even if the attempt frequency were reduced by the same factor as the barrier, to 5 THz, the diffusion coefficient would be 6.0×10^{-7} cm^2/s, still 10^9 times larger than in the neutral cell.

The ability to change the carrier density during device operation by applying a gate voltage is thus an additional remarkable feature of graphene. Manipulating C-O bonding between the extremes of a fast diffusing state, where oxygen atoms experience a low surface corrugation, and a strong epoxy bonding that increases the chances of graphene unzipping opens new avenues for exciting electronic applications, analogous to those reported for carbon nanotubes [44, 45]. The barrier of 0.15 eV is an order or magnitude lower than that determined experimentally for graphite [9] and >5 times lower than the lowest barrier for surface diffusion of O on metals [46]. We thus envision self-assembled patterns of oxygen adsorption; subsequent to oxidation of a graphene sheet, an increased surface mobility should allow the system to relax to patterns that minimize the adsorption energy. As has been discussed recently [7], surface oxygen tends to form specific strips with sp^2 carbon regions in between; after the O atoms are allowed to

equilibrate in such patterns, simple gate-voltage-mediated charge density reduction is expected to fix the pattern into its desired place.

This work was supported by the Donors of the American Chemical Society Petroleum Research Fund, FONDECYT-Chile (project #1080334) and the US-Israel Binational Science Foundation (grant #2006238). Supercomputing facilities used were funded in part by the Materials Simulation Center, a Penn-State MRSEC/MRI facility, and the National Science Foundation (grant OCI-0821527).

---

[1] K. S. Novoselov *et al.*, Nature **438**, 197 (2005).
[2] J. T. Ye *et al.*, Nature Mater. **9**, 125 (2010).
[3] A. Bhattacharya *et al.*, Appl. Phys. Lett. **85**, 997 (2004).
[4] A. K. Geim, Science **324**, 1530 (2009).
[5] A. K. Geim, and K. S. Novoselov, Nature Mater. **6**, 183 (2007).
[6] J.-L. Li *et al.*, Phys. Rev. Lett. **96**, 176101 (2006).
[7] J.-A. Yan, L. Xian, and M. Y. Chou, Phys. Rev. Lett. **103**, 086802 (2009).
[8] I. Jung *et al.*, Nano Lett. **8**, 4283 (2008).
[9] R. Ruoff, Nat. Nanotechnol. **3**, 10 (2008).
[10] S. Ghosh *et al.*, Science **330**, 1656 (2010).
[11] L. R. Radovic, J. Am. Chem. Soc. **131**, 17166 (2009).
[12] R. T. Yang, and C. Wong, J. Chem. Phys. **75**, 4471 (1981).
[13] W. C. Conner, and J. L. Falconer, Chem. Rev. **95**, 759 (1995).
[14] G. M. Pajonk, S. J. Teichner, and J. E. Germain, *Spillover of Adsorbed Species* (Elsevier, Amsterdam, 1983).
[15] S. J. Teichner, Applied Catalysis **62**, 1 (1990).
[16] L. R. Radovic, and F. Rodríguez-Reinoso, in *Chemistry and Physics of Carbon, Vol. 25*, edited by P. A. Thrower (Marcel Dekker, New York, 1997), p. 243.
[17] E. Baumgarten, and L. Maschke, Appl. Catal. A **202**, 171 (2000).
[18] A. Lueking, and R. T. Yang, J. Catal. **206**, 165 (2002).

[19] J. A. Menéndez *et al.*, J. Phys. Chem. **100**, 17243 (1996).
[20] E. Baumgarten, and B. Dedek, React. Kinet. Catal. Lett. **67**, 21 (1999).
[21] E. Baumgarten, and A. Schuck, React. Kin. Catal. Lett **61**, 3 (1997).
[22] H. Boehm, A. Clauss, and U. Hofmann, J. Chim. Phys. Phys.-Chim. Biol. **58**, 141 (1961).
[23] D. Dreyer *et al.*, Chem. Soc. Rev. **39**, 228 (2010).
[24] H. Fidder *et al.*, J. Phys. Chem. A **113**, 6289 (2009).
[25] A. Izuoka *et al.*, Tetrahedron Lett. **38**, 245 (1997).
[26] G. Kresse, and J. Furthmüller, Comput. Mat. Sci. **6**, 15 (1996).
[27] G. Kresse, and J. Furthmüller, Phys. Rev. B **54**, 11169 (1996).
[28] P. E. Blöchl, Phys. Rev. B **50**, 17953 (1994).
[29] G. Kresse, and D. Joubert, Phys. Rev. B **59**, 1758 (1999).
[30] J. P. Perdew, K. Burke, and M. Ernzerhof, Phys. Rev. Lett. **77**, 3865 (1996).
[31] J. P. Perdew, K. Burke, and M. Ernzerhof, Phys. Rev. Lett. **78**, 1396 (1997).
[32] H. J. Monkhorst, and J. D. Pack, Phys. Rev. B **13**, 5188 (1976).
[33] G. Henkelman, and H. Jonsson, J. Chem. Phys. **113**, 9978 (2000).
[34] D. Sheppard, R. Terrell, and G. Henkelman, J. Chem. Phys. **128**, 134106 (2008).
[35] J. Neugebauer, and M. Scheffler, Phys. Rev. B **46**, 16067 (1992).
[36] G. Makov, and M. C. Payne, Phys. Rev. B **51**, 4014 (1995).
[37] The positive counter-charge is modeled as a uniform positive background. As a test of the influence of this approximation, we noticed that for differences in distance from the graphene plane to an oxygen atom in the bridge or the top position, the electrostatic potential change upon charging is minimal.
[38] D. W. Boukhvalov, and M. I. Katsnelson, J. Am. Chem. Soc. **130**, 10697 (2008).
[39] J.-A. Yan, and M. Y. Chou, Phys. Rev. B **82**, 125403 (2010).
[40] G. Glockler, J. Phys. Chem. **62**, 1049 (1958).
[41] M. D. Segall *et al.*, Phys. Rev. B **54**, 16317 (1996).
[42] G. H. Vineyard, J. Phys. Chem. Solids **3**, 121 (1957).
[43] G. Henkelman, VASP TST Tools, http://theory.cm.utexas.edu/vtsttools/dynmat/
[44] V. Derycke *et al.*, Nano Lett. **1**, 453 (2001).
[45] P. G. Collins *et al.*, Science **287**, 1801 (2000).

[46] E. G. Seebauer, and C. E. Allen, Prog. Surf. Sci. **49**, 265 (1995).

TABLE I. Geometries and energy barriers for the different charge densities. The labels correspond to those shown in Fig. 1.

Charge (cm^{-2})	Equilibrium State			Transition State						Energy Barrier (eV)
	P(Å)	CO(Å)	CC(Å)	P(Å)	CO(Å)	CC(Å)	∠CCO1	∠CCO2	∠CCO3	
$+7.64\times10^{13}$	0.52	1.48	1.52	0.50	1.45	1.48	109.5^{O}	98.8^{O}	97.9^{O}	0.89
Neutral	0.52	1.49	1.51	0.53	1.44	1.48	108.1^{O}	101.0^{O}	99.9^{O}	0.73
-3.82×10^{13}	0.52	1.50	1.50	0.60	1.43	1.49	104.8^{O}	104.7^{O}	103.6^{O}	0.45
-7.64×10^{13}	0.56	1.52	1.48	0.67	1.43	1.49	105.6^{O}	105.5^{O}	105.4^{O}	0.15

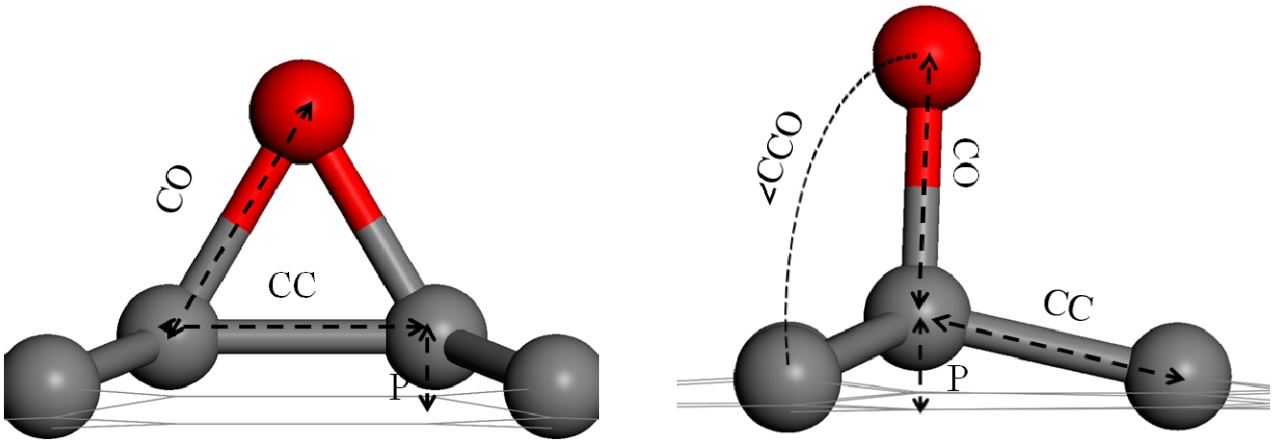

FIG. 1. (color online) Equilibrium (left) and transition (right) state geometry for one oxygen atom (red) adsorbed on graphene (gray). The measurements indicated by the labels are reported in Table I. P represents puckering with respect to the graphene plane.

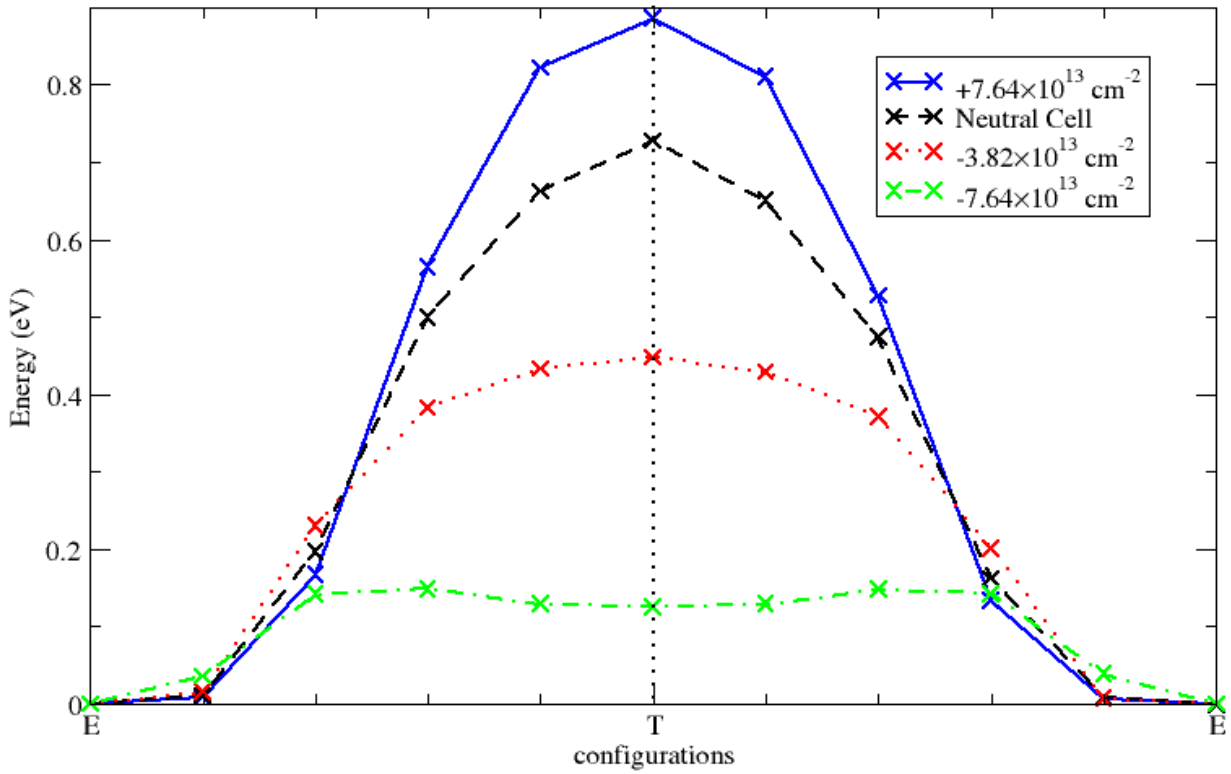

1

2 FIG. 2. (color online) Energies of the different configurations used to determine the transition
3 state. The first and the last configuration correspond to the equilibrium state (E) and the central
4 configuration is the transition state (T). The distance is the same between all images and does not
5 represent the real distance between oxygen positions.

6

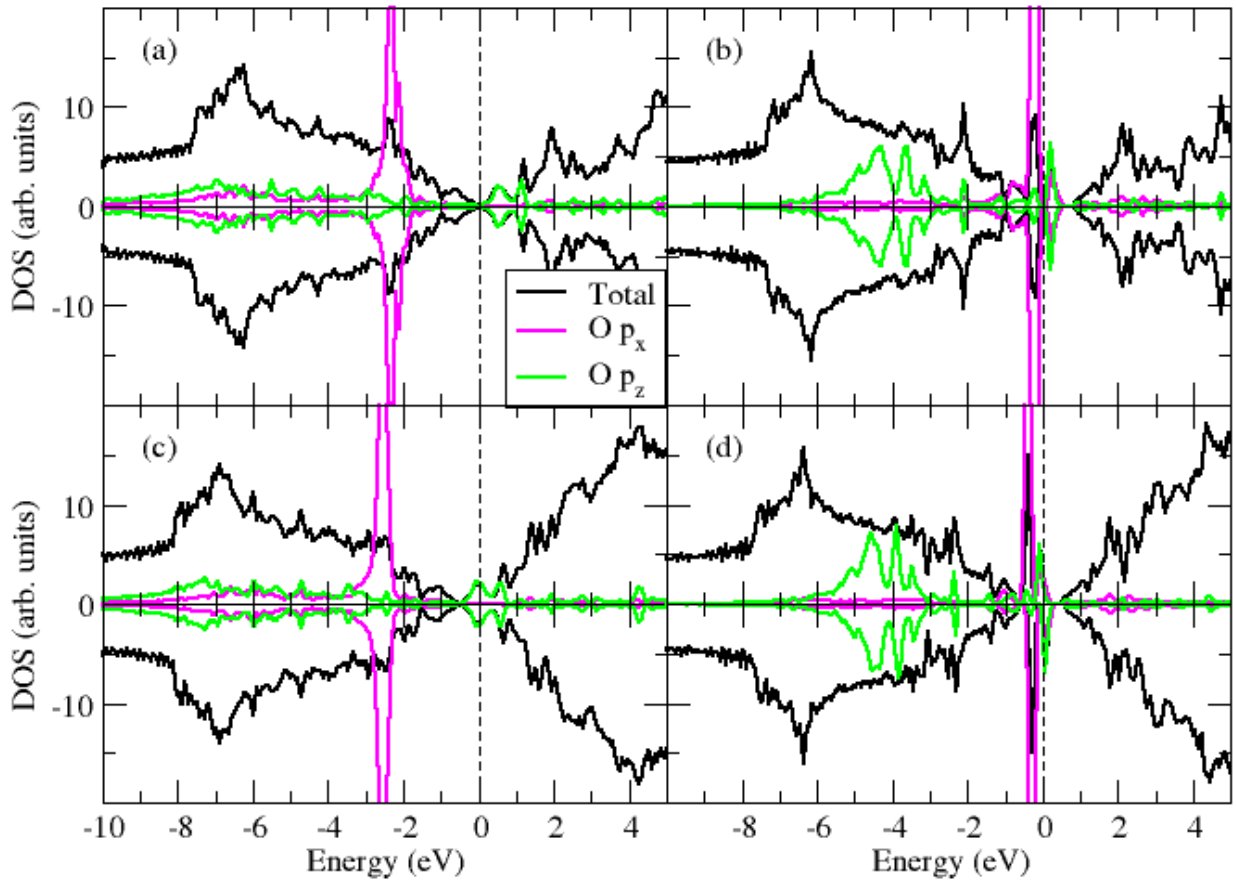

FIG. 3. (color online) Total density of states and the partial densities of states corresponding to the O p_z orbital and the p orbitals parallel to the plane as a function of energy measured from the Fermi level. The left panels correspond to the equilibrium state for the neutral plane (a) and the electron-doped plane with density -7.64×10^{13} cm^{-2} (c). The right panels correspond to the transition state neutral (b) and electron-doped with density -7.64×10^{13} cm^{-2} (d). O projections are rescaled for clarity.